scientific reports

Check for updates

OPEN

Elucidating the anti-fibrotic mechanisms of *Abrus cantoniensis* in hepatic fibrosis using network pharmacology and proteomics

Yang Zheng[1,2], Jiahui Wang[1,2], Liang Liang[1], Yaxuan Qin[1], Lei Wang[1]✉ & Huaye Xiao[1]

This study aimed to elucidate the effects and underlying mechanisms of *Abrus cantoniensis* in treating mice hepatic fibrosis, thereby providing a rationale for its clinical application. To investigate *A. cantoniensis* effects in hepatic fibrosis, we established a carbon tetrachloride-induced mouse model validated by histopathology. Potential active compounds were revealed through LC-MS, and core targets were identified by network pharmacology integrated with proteomics. Validation was performed using molecular docking, molecular dynamics, and immunohistochemistry. Histopathology confirmed the anti-hepatic fibrosis effects of *A. cantoniensis*. The LC-MS analysis identified 420 compounds, while network pharmacology and proteomics revealed 208 and 738 key targets, respectively. Functional enrichment revealed that these targets were involved in hepatic fibrosis-related processes. Intersecting both analyses identified four core targets: BRAF, CDK2, DNMT1, and PDGFRB. Molecular docking and dynamics simulations demonstrated strong and stable binding between the potential active compounds and these targets, which was further validated by immunohistochemistry showing suppressed expression of the targets. Our integrated multi-omics study elucidated that the anti-hepatic fibrosis effect of *A. cantoniensis* was mediated by the core targets BRAF, CDK2, DNMT1, and PDGFRB, thus supporting its development as a standardized phytomedicine.

Keywords Abrus cantoniensis, Hepatic fibrosis, Network pharmacology, Proteomics, DNMT1

Hepatic fibrosis is a global health problem, with approximately 2 million people dying from chronic liver disease each year, accounting for 4% of global deaths[1]. Hepatic fibrosis is a dynamic and reversible pathological process characterized by excessive and dysregulated extracellular matrix (ECM) deposition in the liver[2]. It arises as a compensatory mechanism in response to chronic liver injury, driven by persistent inflammatory stimuli from diverse pathogenic factors. This aberrant ECM accumulation is a critical transitional phase in the progression of chronic liver disease toward cirrhosis[3]. A number of chronic liver injury factors can activate the transformation of hepatic stellate cells into myofibroblasts, which highly express α-smooth muscle actin and cause substantial ECM deposition within the liver; this process is the central mechanism in hepatic fibrosis[4]. Symptoms of hepatic fibrosis are mainly fatigue, dry mouth, visual fatigue, and a bitter taste in the mouth. Currently, drugs used in the clinical treatment of hepatic fibrosis mainly target the initial factors causing chronic liver diseases or one or more mechanistic links that affect hepatic fibrosis. However, there are no interventions for hepatic fibrosis itself that are highly effective, and the efficacy of traditional therapies is limited by significant side effects[5]. Unfortunately, the molecular mechanisms of hepatic fibrosis are complex, and effective diagnostic and therapeutic interventions for hepatic fibrosis remain elusive. Therefore, the development of drugs with fewer adverse effects and a more precise and higher efficacy is the focus of current research.

Abrus cantoniensis was first recorded in the Lingnan Record of Herbal Medicine, and it is mainly distributed in Guangdong, Guangxi, and other places. It is sweet, slightly bitter, cool in nature, and belongs to the liver and stomach meridians. It induces dampness, removes yellow, clears heat, removes toxins, dredges the liver, and relieves pain[6]. *(A) cantoniensis* is a medicinal and edible plant, commonly used clinically to treat liver diseases such as chronic hepatitis (B) Modern pharmacological studies have demonstrated that it exerts various biological functions, including lipid-lowering, liver-protective, anti-inflammatory, analgesic, immune-

[1]Department of Medicine, Faculty of Chinese Medicine Science Guangxi, University of Chinese Medicine, Nanning 530222, Guangxi, China. [2]Yang Zheng and Jiahui Wang contributed equally to this work. ✉email: wl13610222925@163.com

enhancing, and antioxidant effects[7]. *A. cantoniensis* is rich in a variety of chemical compounds, including amino acids, phenolic compounds, cardiac glycosides, triterpenoids, flavonoids, coumarins, alkaloids, phytosterols, and polysaccharides. Among these, alkaloids, flavonoids, and triterpenoids are identified as the primary bioactive constituents of *A. cantoniensis*[8]. Several studies have shown that *A. cantoniensis* has definite anti-hepatic fibrosis and hepatoprotective effects, but the material basis and molecular mechanisms of its action have not been fully elucidated[9,10]. Network pharmacology is an interdisciplinary means of systematically investigating the complex interactions between herbal compounds and biological targets, with a particular emphasis on elucidating the material basis and potential mechanisms underlying traditional Chinese medicine's multi-component, multi-target therapeutic effects. Proteomics is the large-scale study of protein expression, interactions, and modifications. It can help to systematically decipher the molecular mechanisms of traditional Chinese medicine by identifying key pharmacodynamic proteins, signaling pathways, and biological networks affected by herbal compounds. Therefore, in this study, we applied integrated network pharmacology and proteomics to elucidate the anti-hepatic fibrosis mechanisms and potential bioactive constituents of *A. cantoniensis*, providing a scientific foundation for its clinical application.

Materials and methods

Drugs and reagents

A. cantoniensis was purchased from Guangdong Yifang Pharmaceutical Co., Ltd. (Guangdong, China). Silybin was purchased from Tianjin Tianshili Shengte Pharmaceutical Co., Ltd, (Tianjin, China). A hepatic fibrosis four-item kit was purchased from Shanghai Enzyme-Link Biotechnology (Shanghai, China). HE, Masson, and sirius red staining kits were purchased from Beyotime (Shanghai, China). Antibodies against α-SMA, collagen I, and collagen III were purchased from Cell Signaling Technology (Denver, MA, USA). A DAB chromogen kit was purchased from Servicebio (Wuhan, China). A BCA protein quantification kit was purchased from Beyotime (Shanghai, China). Pancreatic enzymes were purchased from Promega (Madison, WI, USA).

Laboratory animals

Male C57BL/6J mice ($n = 30$, 7 weeks old, body weight 20–25 g), purchased from Hunan Silaike Jingda Laboratory Animal Co., Ltd. (Laboratory Animal Production License No. SCXK (Xiang) 2021-0002), were housed at the Animal Experiment Center of Guangxi University of Chinese Medicine (Facility Use License No. SYXK (Gui) 2024-0004). The animals were maintained under specific pathogen-free conditions, with the ambient temperature controlled at 22 ± 3 °C and a 12-h light/dark cycle. Food and water were provided ad libitum throughout the experimental period. The mice were anesthetized by isoflurane inhalation and euthanized by cervical dislocation under anesthesia. All experimental procedures were conducted in compliance with the Guidelines for the Management of Laboratory Animals and were approved by the Institutional Animal Care and Use Committee of Guangxi University of Chinese Medicine (Approval No. DW20241115-SY009). We confirm that the procedures in this study were performed in accordance with the ARRIVE guidelines.

Drug preparation

The medicinal herb *A. cantoniensis* was authenticated as genuine by Associate Professor Maochun Huang, an expert in medicinal botany. Specimens of *A. cantoniensis* were housed at the Chinese Medicinal Herb Specimen Collection of Chengdu University of Chinese Medicine (CDCM0003168). *A. cantoniensis* herb (3 kg) was divided into three equal parts and immersed in 10 times the amount of water for 1 h. The mixture was then boiled for 2 h, and the extract was collected. The herbs were then boiled in five times the amount of water for 1 h. The extract was collected and combined with the filtrate, concentrated to 1.5, 3, or 6 g/mL, and refrigerated (Haier, China) at − 20 °C until use.

Identification of the compounds in *A. cantoniensis*

To prepare *A. cantoniensis*, 100 mg of a sample was weighed, and 500 µL of the extract in methanol (Thermo Fisher Scientific, USA) and water (4:1) was added. The mixture was vortexed for 30 s, sonicated at 45 Hz for 4 min, and then sonicated in an ice water bath for 1 h. The sample was allowed to stand at − 40 °C for 1 h and then centrifuged at 12,000 rpm and 4 °C for 15 min. Finally, the supernatant was precisely pipetted and slowly filtered through a 0.22-µm microporous filter membrane and transferred into liquid chromatography vials for LC-MS (UHPLC-Q-Exactive Orbitrap MS) analysis. Chromatographic separation was achieved on a Waters Acquity UPLC BEH C18 column (Waters, USA) (2.1 mm × 100 mm, 1.7 µm) maintained at 40 °C. The mobile phase consisted of (A) water and (B) acetonitrile, both containing 0.1% formic acid. A gradient elution program was applied as follows: 2% B (0–14 min), increased to 60% B (14–16.5 min), then to 98% B (16.5–18 min), and held at 98% B (18–20 min). The flow rate was 0.3 mL/min, with an injection volume of 5 µL. Mass spectrometric detection was carried out in the positive electrospray ionization mode. The full MS scan (m/z 100–1500) was acquired at a resolution of 70,000, and data-dependent MS/MS scans were acquired at a resolution of 17,500. The capillary and auxiliary gas heater temperatures were both 350 °C. The sheath and auxiliary gas flow rates were 10 and 35 arb, respectively. The spray voltage was 3.0 kV, and stepped collision energies of 20, 30, and 40 eV were used for fragmentation. To identify compounds, raw data were first processed using Progenesis QI software for baseline filtering, peak identification, and peak alignment. Compounds were then characterized by searching the HMDB database (https: www.hmdb.ca/) and METLIN database (http: www.metlin.scripps.edu) based on mass number, secondary fragmentation, and isotopic distribution. The database was accessed at 9:05 on 29 April 2025.

Based on the chromatographic peak areas determined by LC-MS, we performed a relative quantification of the identified compounds. By classifying them according to chemical structure and calculating the percentage of the sum of peak areas within each category relative to the total peak area, we obtained a distribution of the component concentrations by category. A comprehensive LC-MS method was used to systematically analyze

A. cantoniensis constituents. Relative quantification was performed based on chromatographic peak areas, with compound identification achieved by comparing the data against a standard mass spectrometry database (Progenesis QI). Compounds were subsequently classified according to their chemical structures, and the final calculations determined the number of compounds within each category and their respective abundances (%).

Preparation and grouping of the hepatic fibrosis model mice

After 1 week of acclimatization, C57BL/6J mice were randomly divided into six groups ($n = 5$ each): a normal control group; a model control group; low- (15 g/kg), medium- (30 g/kg), and high-dose (60 g/kg) *A. cantoniensis* groups; and a silybin (100 mg/kg) group. Hepatic fibrosis was induced in all groups except the normal control group by intraperitoneal injection of 40% CCl_4 in peanut oil (2 μL/g body weight) twice weekly for 8 weeks. The normal control group received equivalent volumes of peanut oil vehicle. Starting from the fifth week of modeling, the *A. cantoniensis* groups were administered appropriate doses of *A. cantoniensis* via daily oral gavage, while the silibinin group received 100 mg/kg/day silibinin orally. Both were administered at 0.1 mL/10 g body weight. The normal and model control groups received equivalent volumes of saline daily for 4 consecutive weeks.

Liver histopathological tests

The liver tissue of mice in each group were fixed for 48 h, placed in an automatic dehydrator (Leica, Germany) for gradient dehydration, embedded, sectioned (Thermo Fisher Scientific, USA), and deparaffinized according to the instructions provided by the manufacturers of the HE, Masson, and sirius red staining kits. The tissue slices were sealed with neutral gum, and the structure and collagen fiber deposition of liver tissue from each group of mice were observed under a light microscope (Olympus, China).

Liver function tests

The serum alanine aminotransferase (ALT), aspartate aminotransferase (AST), alkaline phosphatase (ALP), and bilirubin levels were assessed in each group of mice using a fully automated biochemical analyzer (Hitachi, Japan).

Hepatic fibrosis four-item test

Mouse liver tissue (0.1 g) was added to 0.9 mL of refrigerated saline to prepare tissue homogenate. The homogenate was centrifuged, and the supernatant was collected. The contents of HA, LN, P-IIIC, and IV-C in the supernatant were analyzed according to the instructions of an ELISA kit.

Network pharmacology analysis

The potential active compounds of *A. cantoniensis* identified by LC-MS were screened by the SwissADEM platform[11] using five druglikeness rules of Lipinski, Ghose, Veber, Egan, and Muegge. The results were all positive, with oral utilization (OB) ≥ 30% and drug-like properties (DL) ≥ 0.18, based on the TCMSP database[12]. The TCMSP and SwissTargetPrediction databases were also used to obtain the targets of the potential active compounds of *A. cantoniensis*. The search term "Hepatic fibrosis" was used to screen the Genecards[13], OMIM[14], and TTD[15] databases (accessed at 10:40 on 1 May 2025) to obtain targets related to hepatic fibrosis. By processing the drug-disease target interactions, key targets were identified. The STRING database (accessed at 11:30 on 1 May 2025)[16] was used to obtain key target interaction relationships, and Cytoscape 3.9 software[17] was used to visualize the protein interaction network. An enrichment analysis of these key targets was performed using the Sanger platform.

Proteomics analysis

Liver tissue samples were collected from the blank group, model group, and medium-dose *A. cantoniensis* group for subsequent proteomics analysis, with four biological replicates per group. The total protein was extracted from each sample. The protein concentration was determined using a BCA assay, with quality control based on SDS-PAGE (Solarbio Life Sciences, China). Subsequently, the protein was subjected to tryptic digestion, and the resulting peptides were desalted and quantified.

Finally, the peptide samples were analyzed using a Vanquish™ Neo UHPLC system coupled to an Astral mass spectrometer for data-independent acquisition (DIA).

The lyophilized sample was reconstituted in 10 μL of aqueous 0.1% formic acid (mobile phase A) and centrifuged at 14,000×g and 4 °C for 20 min. A 200-ng aliquot of the supernatant was injected for analysis. LC-MS/MS analysis was performed on a Vanquish Neo nanoflow UHPLC system coupled online to an Orbitrap Astral mass spectrometer (Thermo Fisher Scientific). Chromatographic separation was achieved using a C18 pre-column (5 mm × 300 μm, 5 μm, Thermo) and a PepMap™ Neo C18 analytical column (150 μm × 15 cm, 2 μm, Thermo) maintained at 50 °C. The mobile phase consisted of 0.1% formic acid in water (A) and 0.1% formic acid in 80% acetonitrile (B). Details of the gradient elution program are provided in Supplementary Table 1. The mass spectrometer was equipped with an EASY-Spray ion source operated in positive DIA mode. The mass spectrometer was operated at a spray voltage of 2.0 kV and an ion transfer tube temperature of 290 °C. Full MS1 scans were acquired over a range of m/z 380–980 at a resolution of 240,000 (at m/z 200), with the automatic gain control target set to 500%. For DIA, 300 isolation windows of 2 THz were used with a normalized collision energy of 25%. MS2 scans were acquired over an m/z range of 150–2000 at a resolution of 80,000 on the Astral detector, with a maximum injection time of 3 ms.

The SpectronautTM18 software system was used to establish a mouse protein database, and Meguiar's cloud platform (cloud.majorbio.com) was used for bioinformatics analysis. The t.test function in the R language was used to calculate the P-value of the difference between groups and the multiplicity of difference (FC). Significance was tested at $P < 0.05$, while proteins with a multiplicity of difference greater than 1.2-fold were

considered as differentially expressed proteins (DEPs). The DEPs were analyzed for functional enrichment and further screened for core targets using machine learning.

Integrated analysis

The targets obtained from the network pharmacology analysis were interacted with the targets from the proteomics analysis. The importance of the targets was further analyzed using the random forest method and the degree values in the PPI network of the targets. The target rankings in both cases were summed, and the top four targets were identified as the core targets. A network diagram of the four core targets with the potential active compounds was generated. The SDF files of the potential active compounds were obtained from the PubChem database (accessed at 14:10 on 10 June 2025)[18], and the PDB files of the targets were obtained from the UniProt database (accessed at 14:35 on 10 June 2025)[19]. Molecular docking was carried out using Discovery Studio software, and the results were visualized by PyMOL software. The PDB files of the docking results were imported into the WeMol online platform for 100-ns molecular dynamics simulations.

Immunohistochemistry

Mouse liver tissue was collected from each group, sectioned (thickness of 3 μm), and routinely dewaxed to water. Next, the sections were autoclaved in a sodium citrate solution at 100 °C for 10 min for antigen repair, washed, and blocked in 10% bovine serum albumin for 20 min. A diluted primary antibody was dropped onto the tissue, which was incubated at 4 °C overnight. Next, the tissue sections were incubated in a secondary antibody (Boster, China) for 30 min. The sections were washed, a DAB color development solution was added, the hematoxylin was restained, and the slices were sealed with neutral gum resin (Sionpharm, China). The liver tissue sections were observed under a light microscope (Olympus, China), and semi-quantitative analysis was performed using ImageJ software.

Statistical analysis

IBM SPSS Statistics 25 was used for the statistical analysis (IBM, NY, USA). The data are expressed as mean and standard deviation (SD). One-way or two-way analysis of variance was used to compare the groups, followed by Bonferroni post-hoc analysis. $P < 0.05$ was considered as statistically significant.

Results

A. cantoniensis attenuates CCl_4-induced hepatic fibrosis

We used the classical model of hepatic fibrosis in which mice are induced by intraperitoneal injection of CCl_4. HE staining showed that the hepatocytes of the mice in the blank group were intact and evenly arranged in a radial pattern with the central vein as the center, and the hepatic lobules were structurally intact. In contrast, the hepatic lobules of the mice in the model group were structurally disordered, with interstitial fibrous deposition in the confluent area, fibrous tissue of the confluent area extended into the lobules, and extensive bridging fibrosis. Notably, the interstitial fibrous deposition and bridging fibrosis were improved to varying degrees by intervention with *A. cantoniensis* and silybin. The Masson and sirius red staining results showed that the liver tissue of the mice in the blank group had a clear hepatic lobular structure, with no collagen fiber proliferation present around the liver tissue. However, an increasing number of collagen fibers were seen in the liver tissue of the mice in the model group, whereas the area of collagen fiber deposition was reduced to varying degrees with *A. cantoniensis* and silybin intervention, as shown in Fig. 1a. Liver function tests revealed that ALT, AST, ALP, and bilirubin levels were significantly increased in the model group compared with the control group, and they were significantly decreased in the *A. cantoniensis* groups and silybin group compared with the model group, as shown in Fig. 1b. The hepatic fibrosis four-item kit revealed that HA, LN, P-IIIC, and IV-C were significantly increased in the model group compared with the control group, and they were significantly decreased in the *A. cantoniensis* groups and the silybin group compared with the model group, as shown in Fig. 1c. Immunohistochemistry revealed that the levels of α-SMA, collagen I, and collagen III significantly increased in the model group compared with the control group, and the expression of α-SMA, collagen I, and collagen III significantly decreased in the *A. cantoniensis* groups and the silybin group compared with the model group, as shown in Fig. 1d. In conclusion, *A. cantoniensis* clearly demonstrated anti-hepatic fibrosis effects.

Screening of *A. cantoniensis* active compounds

LC-MS analysis coupled with library matching identified 420 compounds in *A. cantoniensis* (see Supplemental File excel 1 for details). These compounds included 137 and 283 compounds identified in negative and positive ion modes, respectively. The main high-abundance compounds were alkaloids and their derivatives, amino acids and analogs, and flavonoids, with flavonoids and terpenoids being the most abundant classes (Fig. 2a, b). Preliminary screening using the SwissADEM platform and all five rules of Lipinski, Ghose, Veber, Egan, and Muegge in druglikeness yielded 101 compounds. Further screening based on OB and DL in the TCMSP database yielded 27 potential active compounds (see Supplemental File excel 2 for details) of *A. cantoniensis*, as detailed in Fig. 2c, d.

Network pharmacology-based exploration of the anti-hepatic fibrosis mechanism of *A. cantoniensis*

Using the search term "Hepatic fibrosis," 2608, 197, and 18 hepatic fibrosis-related targets were obtained from Genecards, OMIM, and TTD databases, respectively. After merging and de-duplication, 2704 hepatic fibrosis-related targets were retained. Additionally, 497 potential active compounds of *A. cantoniensis* were identified using the TCMSP and SwissTargetPrediction databases. The drug targets and disease-related targets were processed interactively to obtain 208 key targets of *A. cantoniensis* in the prevention and treatment of hepatic

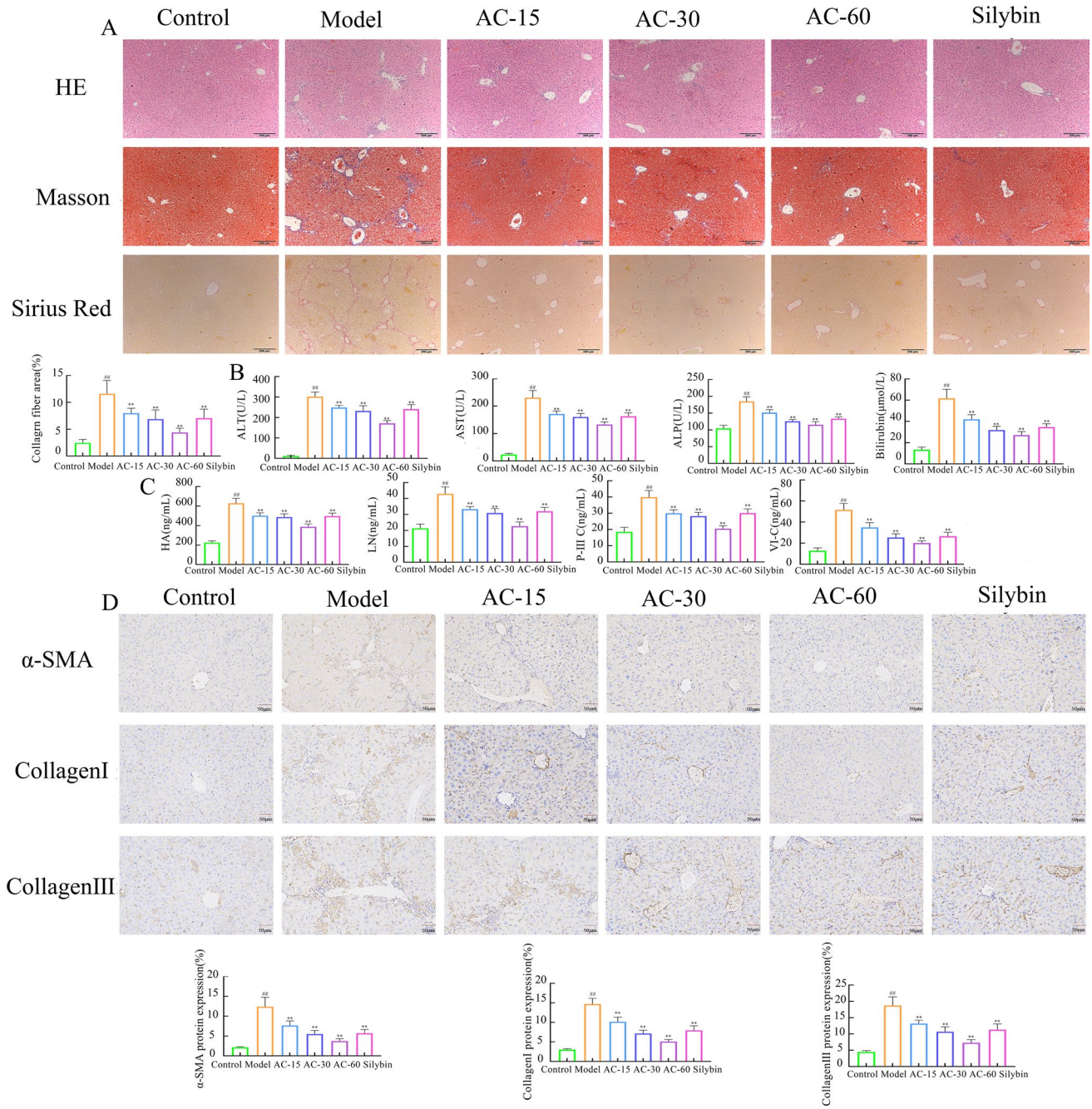

Fig. 1. *A. cantoniensis* attenuates CCl_4-induced hepatic fibrosis. (**a**) HE, Masson, and sirius red staining of liver tissue; bar = 200 μm. (**b**) Serum levels of ALT, AST, ALP, and bilirubin. (**c**) HA, LN, P-IIIC, and IV-C content in liver tissue homogenates. (**d**) Protein levels of α-SMA, collagen I, and collagen III; bar = 50 μm. Data in each panel are expressed as mean ± SD; $^{\#}P < 0.05$ versus control, $^{\#\#}P < 0.01$ versus control, $^{*}P < 0.05$ versus model, $^{**}P < 0.01$ versus model. Note: AC-15: *Abrus cantoniensis*, 15 g/kg; AC-30: *Abrus cantoniensis*, 30 g/kg; AC-60: *Abrus cantoniensis*, 60 g/kg.

fibrosis, as shown in Fig. 3a. Protein interactions were analyzed for the 208 key targets, which produced a total of 208 nodes and 6920 edges, as detailed in Fig. 3b. The mean values of the network's topological parameters were as follows: degree centrality, 33.269; betweenness centrality, 4.535×10^{-3}; and closeness centrality, 0.515 (see Supplemental File excel 3 for details). The total number of gene functions and that of pathways identified were 1,075 and 265, respectively (see Supplemental Files excel 4 and excel5 for details). A gene function and pathway enrichment analysis of the key targets revealed that the molecular functions mainly included ATP binding, nuclear receptor activity, transcriptional coactivator binding, histone deacetylase binding, and iron ion binding. The biological processes included the vascular endothelial growth factor signaling pathway, positive regulation of transcription by RNA polymerase II, inflammatory response, angiogenesis, positive regulation of

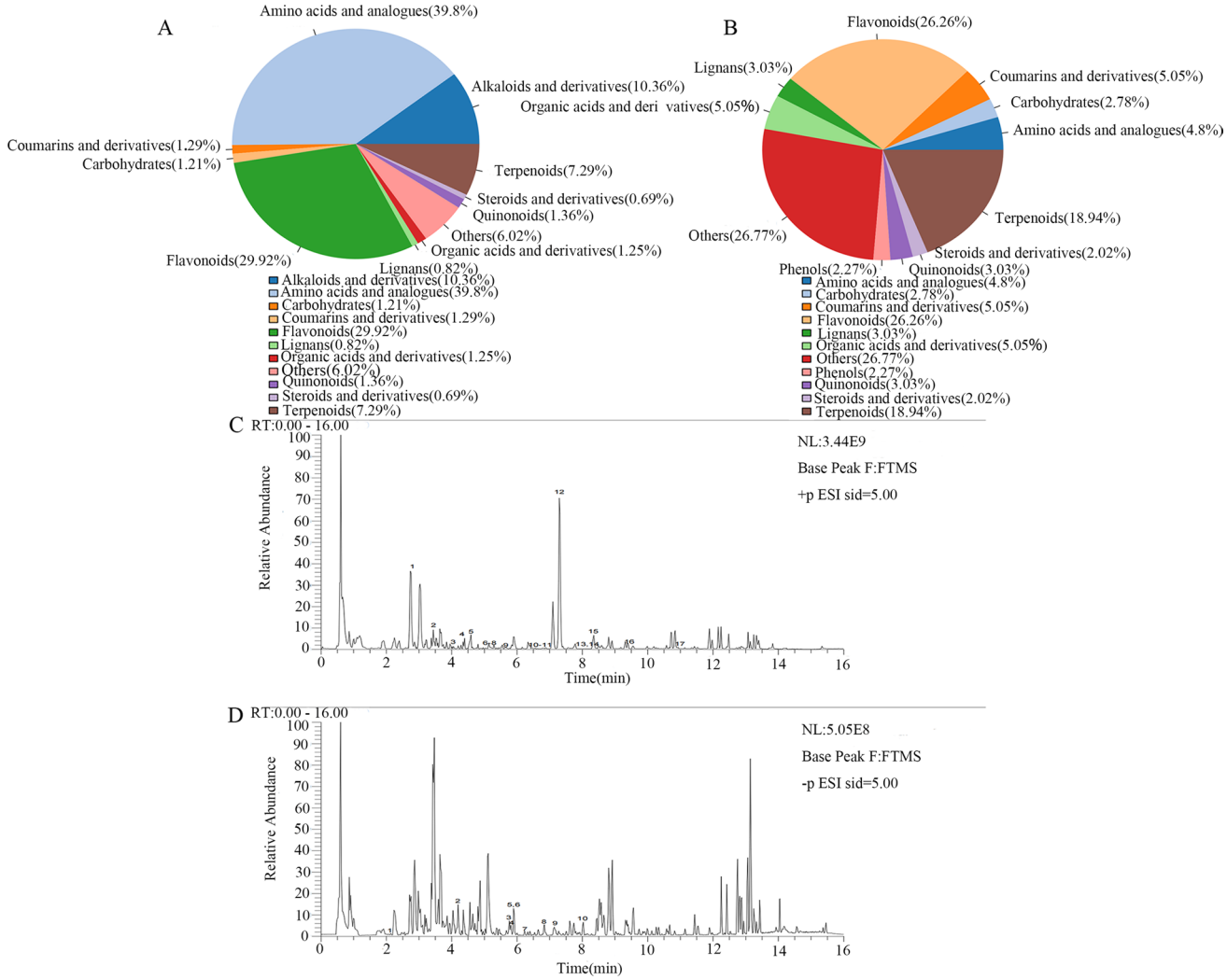

Fig. 2. Screening of potential active compounds of *A. cantoniensis*. (**a**) Pie chart of the content of *A. cantoniensis*. (**b**) Pie chart of the number of compounds of *A. cantoniensis*. (**c**) Potential active compounds screened in the positive ion mode. 1: L-abrine; 2: epicatechin; 3: 3-hydroxyflavone; 4: ammothamnine; 5: glycitein; 6: ailanthone; 7: scoparone; 8: aurantio-obtusin; 9: luteolin; 10: abscisic acid; 11: biochanin A; 12: irigenin; 13: tectochrysin; 14: liquiritigenin; 15: citropten; 16: oroxylin A; 17: piperine. (**d**) Potential active compounds screened in the negative ion mode. 1: ganhuangenin; 2: taxifolin; 3: quercetin; 4: calycosin; 5: sebacic acid; 6: hesperetin; 7: isorhamnetin; 8: licochalcone B; 9: (-)-epiafzelechin; 10: isoliquiritigenin.

apoptosis, endothelial cell migration, glucose metabolism, and positive regulation of NF-κB transcription factor activity. Cellular components included plasma membrane, cytoplasm, extracellular space, cell surface, nucleus, endoplasmic reticulum membrane, and lysosomes. The main pathways were signaling pathways, such as PI3K-AKT, MAPK, apoptosis, HIF-1, FOXO, autophagy, cellular senescence, NF-κB, P53, and linoleic acid, as detailed in Fig. 3c, d.

Proteomics-based Elucidation of the anti-hepatic fibrosis mechanism of *A. cantoniensis*

To further elucidate the mechanism of the anti-hepatic fibrosis action of *A. cantoniensis*, we selected the blank group, the model group, and the medium-dose group for proteomics analysis. The quality of proteomics data can be assessed at both the peptide and protein levels. In this study, a total of 101,843 peptides and 8003 proteins were identified (FDR < 1%) (see Supplemental File txt1 for details), as shown in Fig. 4a The peptide lengths were mainly 7–30 amino acid residues. The peptide length distributions identified by mass spectrometry conformed to the general pattern determined by enzymatic digestion and mass spectrometry fragmentation patterns. They also conformed to quality control requirements, as shown in Fig. 4b. Upregulated differentially expressed proteins were identified according to a fold-change (FC) > 1.5 with $P < 0.05$, and downregulated differentially expressed proteins were identified by FC < 0.67 with $P < 0.05$. There were 738 differentially expressed proteins between the *A. cantoniensis* group and the model group, including 615 downregulated proteins and 123 upregulated proteins, as shown in Fig. 4c. There were a total of 292 and 177 gene functions and pathways identified, respectively (see Supplemental Files excel6 and excel7 for details). Biological processes associated with the differentially

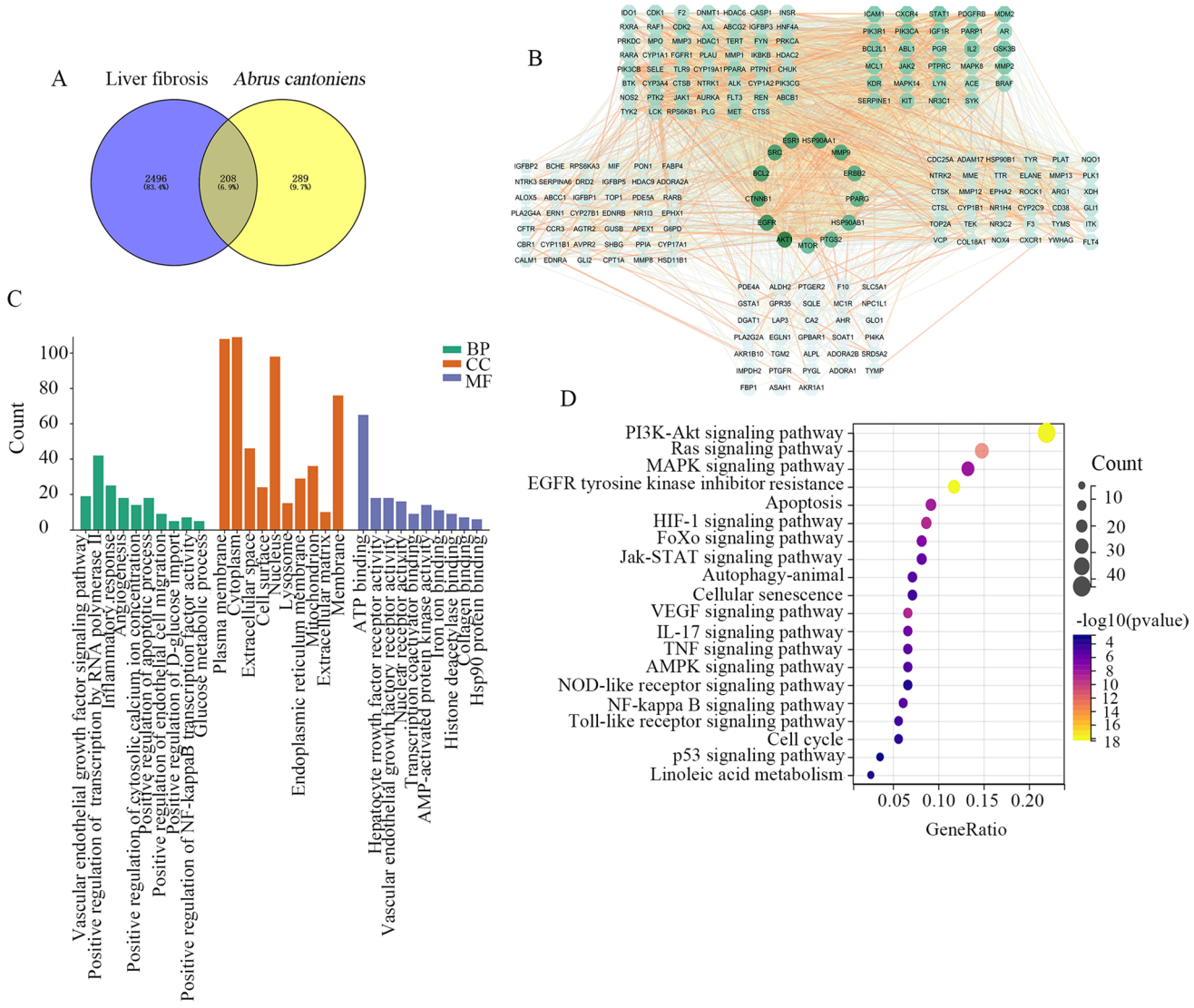

Fig. 3. Network pharmacology analyzes potential mechanisms of anti-hepatic fibrosis. (**a**) *A. cantoniensis* targets of action interact with hepatic fibrosis targets. (**b**) Protein interaction network; the darker the color, the higher the degree value. (**c**) Functional enrichment analysis of key targets. (**d**) Pathway enrichment analysis of key targets.

expressed proteins were mainly enriched in DNA replication, signaling, cellular response to stimuli, glucose metabolic processes, activation of immune responses, redox processes, nucleoside diphosphate phosphorylation, glycolytic processes, and gluconeogenesis. Cellular components were mainly located in the extracellular matrix, extracellular region, and actin complexes. Molecular functions were mainly enriched in calcium ion binding, iron ion binding, heme binding, phosphoenolpyruvate carboxykinase activity, and insulin receptor binding, as detailed in Fig. 4d. The differentially expressed proteins were mainly enriched in steroid biosynthesis, terpene skeleton biosynthesis, type 2 diabetes, drug metabolism—cytochrome P450, central carbon metabolism in cancer, glycolysis and gluconeogenesis, leukocyte migration across the endothelium, Fcγ receptor-mediated phagocytosis, natural killer cell-mediated cytotoxicity, complement and coagulation cascade reactions, cell adhesion molecules, diabetic complications in the AGE-RAGE signaling pathway, chemokine signaling pathway, and regulation of the actin cytoskeleton, as shown in Fig. 4e.

Analysis of the network Pharmacology combined with proteomics

To further obtain the core targets of *A. cantoniensis* in the prevention of hepatic fibrosis, we intersected the key targets obtained by the network pharmacology analysis with those obtained by proteomics to obtain 14 core targets, as shown in Fig. 5a. An importance analysis of the core targets was performed using the machine learning random forest method, as shown in Fig. 5b. To analyze the interactions of the core targets, a protein interaction network was established with 11 nodes and 30 edges, as shown in Fig. 5c. Combining the random forest importance ranking and PPI network degree value ranking, a combined target ranking using both methods was summed, with a higher ranking indicating a more important target. The results showed that CDK2,

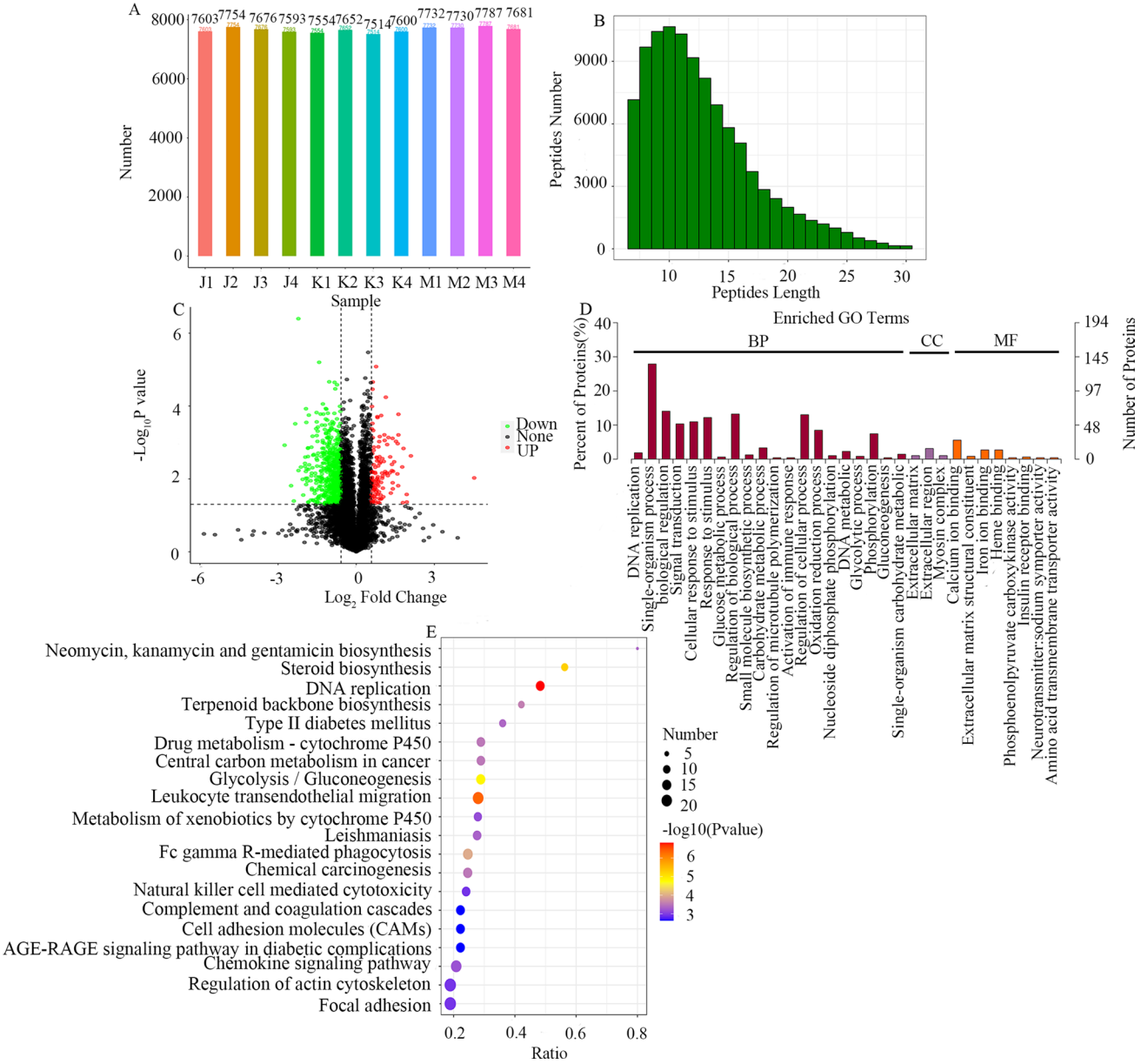

Fig. 4. Proteomics elucidated the molecular mechanism of *A. cantoniensis* in hepatic fibrosis. (**a**) Sample protein identification overview. (**b**) Distribution of peptide lengths. (**c**) Volcano plot of differentially expressed proteins between the *A. cantoniensis* group and the model group. (**d**) Differentially expressed protein function enrichment analysis. (**e**) Differential protein pathway enrichment analysis. Note: K1, normal1; K2, normal2; K3, normal3; K4, normal4; M1, model1; M2, model2; M3, model3; M4, model4; J1, medium-dose *Abrus cantoniensis* 1; J2, medium-dose *Abrus cantoniensis* 2; J3, medium-dose *Abrus cantoniensis* 3; J4, medium-dose *Abrus cantoniensis* 4.

DNMT1, BRAF, and PDGFRB were the key targets. To assess the trend in the expression of the four core targets in the *A. cantoniensis* group compared to the model group and further determine the function of the four core targets in the disease process, we analyzed the results using proteomics. The results revealed that the expression of all four core targets significantly decreased in the *A. cantoniensis* group, as shown in Fig. 5d.

Molecular docking and molecular dynamics of the core targets and potential active compounds

To evaluate the target binding of the core targets and potential active compounds, we constructed network diagrams corresponding to the four core targets and potential active compounds, as shown in Fig. 6a. We performed molecular docking according to the correspondence. The docking activity was presented in the form of a heatmap, as shown in Fig. 6b. We chose the best docking results of the four core targets for visualization, which were licochalcone B and BRAF (PDB ID: 8VSO), L-abrine and CDK2 (PDB ID: 6Q4G), hesperetin and

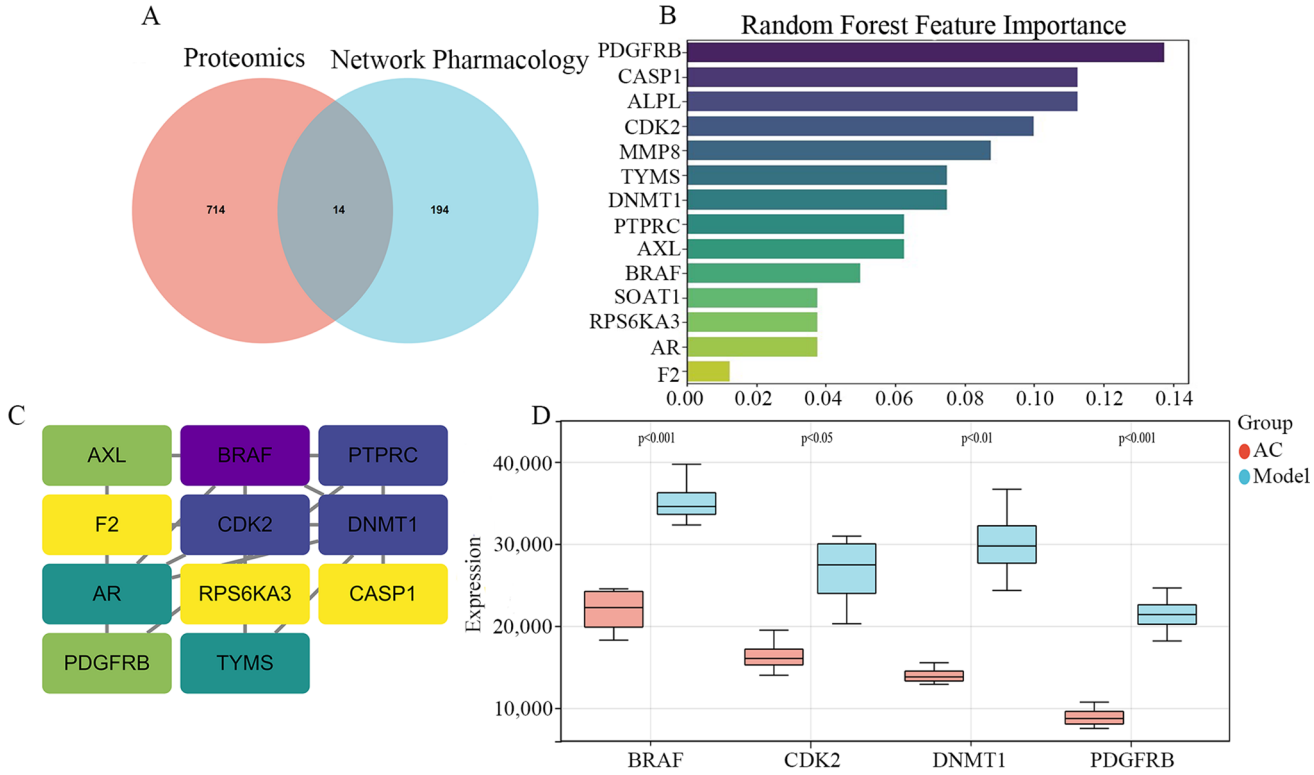

Fig. 5. Combined network pharmacology and proteomics results. (**a**) Venn diagram of the common targets of network pharmacology and proteomics. (**b**) Importance of using the random forest method to analyze core targets. (**c**) Interaction network of the core targets. (**d**) Trends in the expression of the four core targets. Note: AC, *Abrus cantoniensis*..

DNMT1 (PDB ID: 3OS5), and piperine and PDGFRB (PDB ID: 3MJG). The docking scores were − 9.53, − 11.19, − 8.63, and − 11.94 kcal/mol, respectively. All compounds exhibited strong binding affinities, with interaction energies of − 33.11, − 35.03, − 38.36, and − 30.24 kcal/mol, respectively, as detailed in Fig. 6c–f. During the molecular docking between BRAF and licochalcone B, conventional hydrogen bonds were formed between TYR B:19 and GLU C:20. A pi-cation interaction occurred with ARG B:18, and a pi-alkyl interaction was observed with VAL B:51. Multiple residues, including ALA C:58, GLU B:17, ASN B:50, GLY B:54, VAL B:52, GLN B:55, GLU B:20, GLY C:54, GLN C:55, and VAL C:51, participated in van der Waals interactions. During the molecular docking between CDK2 and L-abrine, van der Waals interactions were formed with LEU A:148, ILE A:52, GLY A:147, CYS A:118, PHE A:80, HIS A:60, ASN A:59, PHE A:117, and ALA A:144. Conventional hydrogen bonds formed with VAL A:64, LEU A:66, PHE A:146, and ASP A:145. Pi-alkyl interactions occurred with LYS A:65, VAL A:123, LEU A:58, and LEU A:55. A pi-sigma interaction was generated with ILE A:63, and an unfavorable acceptor-acceptor interaction was observed with LEU A:143. During the molecular docking between DNMT1 and hesperetin, conventional hydrogen bonds were formed with CYS A:288 and GLU A:228. Carbon-hydrogen bonds were observed with GLU A:212 and ASP A:209, while van der Waals interactions involved ALA A:289, PRO A:208, SER A:290, SER A:213, VAL A:216, and LYS A:233. Pi-sigma interactions occurred with LEU A:291, TYR A:284, and VAL A:218. During the molecular docking between PDGFRB and piperine, conventional hydrogen bonds were formed with GLY A:51 and SER B:50. A pi-anion interaction was observed with GLU A:21, and an alkyl interaction was found with CYS A:60. Multiple residues participated in van der Waals interactions, including CYS A:52, VAL B:22, VAL A:22, SER A:50, THR B:20, THR A:20, GLU B:21, ARG B:19, CYS A:49, and ARG A:19. The binding stability was then verified using molecular dynamics simulations, in which the docking products were subjected to simulations for a duration of 100 ns and a step size of 0.002 ns. BRAF and licochalcone B began to stabilize after 40 ns, with a fluctuation range of about 0.35–0.500 nm. CDK2 and L-abrine began to stabilize after 80 ns, with a fluctuation range of about 0.30–0.35 nm, and DNMT1 and hesperetin began to stabilize after 25 ns, with a fluctuation range of about 0.30–0.40 nm. PDGFRB and piperine began to stabilize after 20 ns, with a fluctuation range of about 0.30–0.70 nm. The fluctuation range of all docking simulations was less than 0.5 nm, indicating that the systems reached equilibrium, as detailed in Fig. 6g, j. The peaks in the RMSF indicated that these regions fluctuated the most throughout the simulation. The range of this value for the four pairs of core constituents was between 0.10 Å and 0.90 Å, indicating that the four pairs of core constituents were very stable at specific pressures and temperatures, as detailed in Fig. 6k–n. The radius of gyration measures the compactness of a protein, with a lower value indicating a more tightly folded protein. BRAF and licochalcone B began to stabilize after 60 ns, with a fluctuation range of approximately 2.80–2.90 nm; CDK2 and L-abrine began to stabilize after 20 ns, with a fluctuation range of approximately 2.00–2.06 nm; DNMT1 and hesperetin

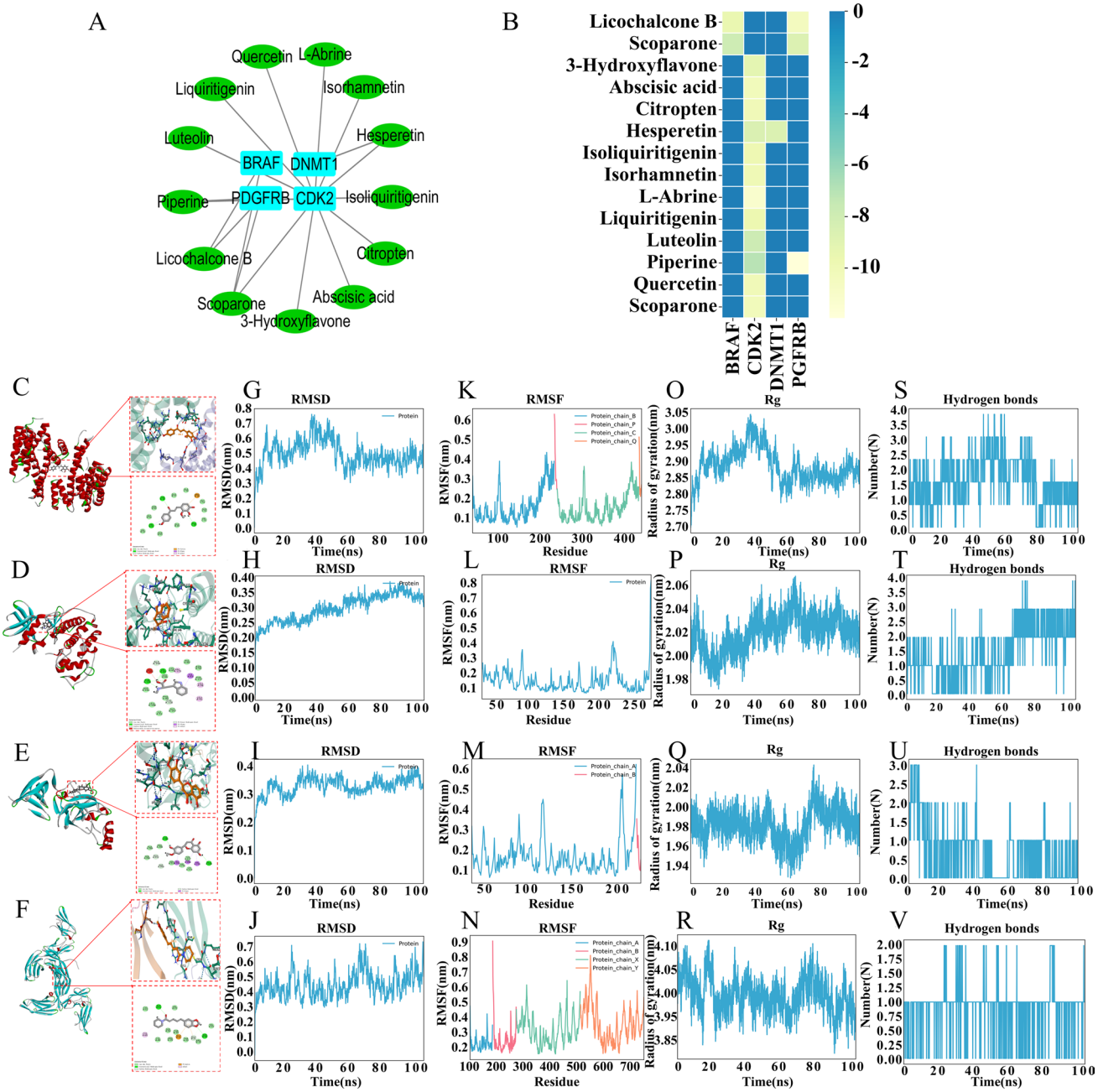

Fig. 6. Analysis of binding viability and stability of core targets with the potential active compounds. (**a**) Network diagram of the relationship between the core targets and their corresponding active compound. (**b**) Heat map of the molecular docking results of the core targets and their corresponding active compound. (**c**) Optimized conformation after docking BRAF with licochalcone B. (**d**) Optimized conformation after docking CDK2 with L-abrine. (**e**) Optimized conformation after docking DNMT1 with hesperetin, (**f**) Optimized conformation of PDGFRB after docking with piperine. (**g**) RMSD curve of BRAF and licochalcone B. (**h**) RMSD curve of CDK2 and L-abrine. (**i**) RMSD curve of DNMT1 and hesperetin. (**j**) RMSD curve of PDGFRB and piperine. (**k**) RMSF curve of BRAF and licochalcone B. (**l**) RMSF curve of CDK2 and L-abrine. (**m**) RMSF curve of DNMT1 and hesperetin. (**n**) RMSF curve of PDGFRB and piperine. (**o**) Rg curve of BRAF and licochalcone B. (**p**) Rg curve of CDK2 and L-abrine. (**q**) Rg curve of DNMT1 and hesperetin. (**r**) Rg curve of PDGFRB and piperine. (**s**) H-bond curve of BRAF and licochalcone B. (**t**) H-bond curve of CDK2 and L-abrine. (**u**) H-bond curve of DNMT1 and hesperetin. (**v**) H-bond curve of PDGFRB and piperine.

began to stabilize after 5 ns, with a fluctuation range of approximately 1.94–2.04 nm; and PDGFRB and piperine began to stabilize after 20 ns, with a fluctuation range of approximately 3.90–4.05 nm. After these time points, the radius of gyration decreased and stabilized, indicating that the protein structure became more compact after ligand binding, which further demonstrated the stability of the protein-ligand complex, as detailed in Fig. 6o, r.

Hydrogen bonds are an important stabilizing factor in protein-ligand interactions. The time to stabilization and the number of hydrogen bonds in the complexes were follows: between BRAF and licochalcone B, 80 ns, with a maximum of five bonds but generally one; between CDK2 and L-abrine, 60 ns, with a maximum of four bonds but typically two; between DNMT1 and hesperetin, 5 ns, with a maximum of three bonds but generally one; and between PDGFRB and piperine, 1 ns, with a maximum of two bonds but typically one. This indicated that stable hydrogen bond interactions were formed between the proteins and ligands, as detailed in Figs. 6S–6 V.

Immunohistochemical analysis of core target expression

To further clarify the effects of *A. cantoniensis* on the four core targets, the medium-dose group of *A. cantoniensis* was selected for validation. The results of immunohistochemistry showed that the expression of the four core targets, CDK2, DNMT1, BRAF, and PDGFRB, was significantly higher in the model group than in the blank group, but it was significantly lower in the *A. cantoniensis* group than in the model group, as shown in Fig. 7. These results were consistent with the proteomics results.

Discussion

Hepatic fibrosis is a key process in the pathology of liver disease, and it is closely related to its progression. Hepatic fibrosis usually develops from a recurrent healing process due to chronic liver injury, such as viral, drug-induced, toxic, metabolic, cholestatic, or autoimmune damage[20]. As the exact pathogenesis is still unclear, the clinical management of hepatic fibrosis mainly focuses on controlling the primary pathogenesis or treating hepatic fibrosis itself[21]. Therefore, mining key targets in the pathogenesis of hepatic fibrosis using a multidisciplinary approach is important for targeted drug development. In recent years, Chinese medicine has achieved remarkable efficacy in preventing and treating hepatic fibrosis[22]. *A. cantoniensis* is one of the "10 geo-authentic crude drugs," which are characteristic local and regional medicinal herbs of Guangxi, and they have shown potential for treating chronic liver disease in modern pharmacological research[23]. Chinese medicines are rich resources, and it is important to search for novel and effective anti-hepatic fibrosis natural drugs using both histological research methods and multi-omics-based systems biology approaches.

In this study, a hepatic fibrosis mouse model was replicated by intraperitoneal injection of CCl_4, which strongly induces hepatic lipid peroxidation, leading to free radical metabolism disorders. This disrupts the normal liver structure and function, causing structural disorders of the hepatic lobules, swelling and necrosis of hepatocytes, and eventually hepatic fibrosis or even cirrhosis with prolonged exposure[24]. Silybin inhibits the activation of hepatic stellate cells in the liver, reduces the expression of HA and other indicators of the degree of hepatic fibrosis, and reduces hepatocellular damage, thus inhibiting hepatic fibrosis. Therefore, in this study, we chose silybin as a positive control for the animal experimental study[25]. Pathological tests and molecular biology experiments have revealed that *A. cantoniensis* has clear anti-hepatic fibrosis effects. To clarify the material basis of the pharmacological effects exerted by *A. cantoniensis*, LC-MS analyses were carried out and 420 potential active compounds were identified. The classes of compounds with higher content and number of different compounds included alkaloids and their derivatives, flavonoids, and terpenoids, which was consistent with the results of previous reports[26].

A network pharmacological analysis identified 208 key anti-hepatic fibrosis targets of *A. cantoniensis*, and a functional enrichment analysis revealed that these targets were primarily related to ATP binding, nuclear receptor activity, iron binding, inflammatory response, angiogenesis, and apoptosis functions. The main related signaling pathways were PI3K-AKT, MAPK, apoptosis, HIF-1, FOXO, autophagy, cellular senescence, NF-κB, and P53, and linoleic acid. Ferroptosis of hepatic stellate cells induced by iron overload was shown to effectively reduce extracellular matrix deposition and exert anti-hepatic fibrosis effects[27]. Pathological vascular neovascularization mediated by hepatic sinusoidal endothelial cells is an early pathological change found in hepatic fibrosis, with HIF-1a inhibiting hepatic vascular neovascularization by affecting the transcription of vascular endothelial growth factor[28]. FOXO1 was shown to mediate hepatic stellate cell activation through the TGF-β1/smad signaling pathway and contribute to the pathological progression of hepatic fibrosis in mice[29]. Autophagy was reported to promote NF-κB-regulated hepatocyte apoptosis, which enhanced hepatic fibrosis and may be a potential therapeutic target of hepatic fibrosis[30]. Cellular senescence is the ultimate cellular fate of proliferating cells undergoing irreversible cell cycle arrest. Senescent hepatic stellate cells exhibit reduced collagen production and proliferation. Thus, induction of senescence may be a protective mechanism against the progression of hepatic fibrosis[31]. Here, a proteomics analysis identified 738 key targets of *A. cantoniensis* in the treatment of hepatic fibrosis, and a functional enrichment analysis revealed that these targets mainly functioned in DNA replication, cellular response to stimuli, gluconeogenesis, glycolytic processes, gluconeogenesis, calcium ion binding, iron ion binding, heme binding, and phosphoenolpyruvate carboxykinase activity. The main pathways of the targets included steroid biosynthesis, glycolysis and glycogenesis, leukocyte transendothelial migration, Fcγ receptor-mediated phagocytosis, natural killer cell-mediated cytotoxicity, cellular adhesion molecules, diabetic complications in the AGE-RAGE signaling pathway, the chemokine signaling pathway, and regulation of the actin cytoskeleton. Calcium ions regulate hepatic stellate cell activation by modulating endoplasmic reticulum stress[32]. Glycolytic reprogramming is a source of energy during hepatic stellate cell activation, and therefore, inhibiting hepatic stellate cell glycolysis may attenuate hepatic fibrosis[33]. Fcγ receptor-mediated phagocytosis is resistant to inflammation and hepatic fibrosis, and thus, it provides a potential therapeutic approach for patients with chronic liver disease[34]. Additionally, natural killer cell exosomes inhibit hepatic stellate cell activation and CCl_4-induced hepatic fibrosis[35]. Notably, there were differences in the GO and KEGG analyses of the key targets in the network pharmacology and proteomics analyses. One key reason is the limited data sources available for use in network pharmacology, and another is that histological techniques provide a large amount of differential expression data, which inevitably leads to differences in results[36]. Undoubtedly, the results of these discrepancies can be used to identify key targets and gain valuable insights from data with complete background information

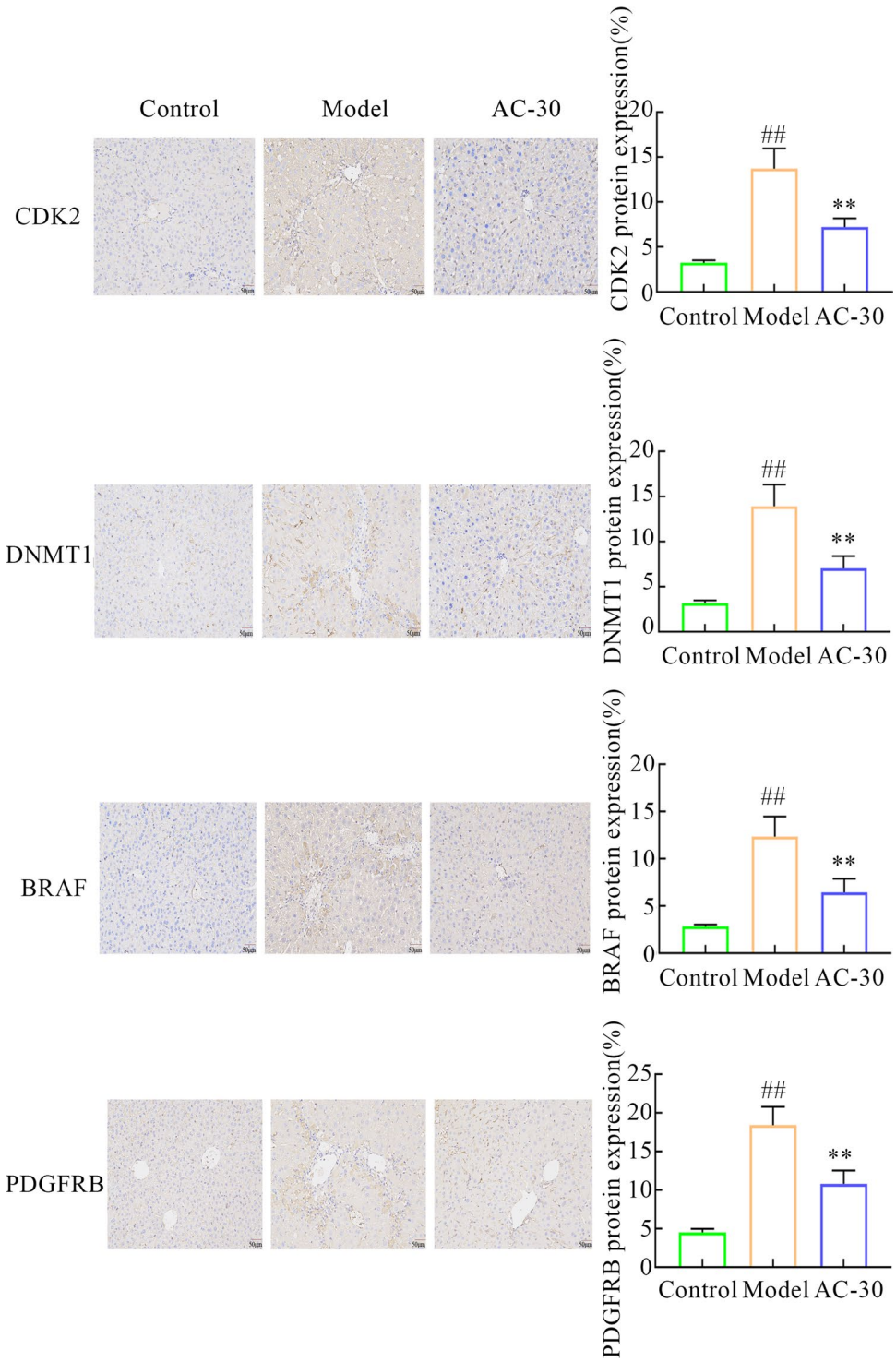

Fig. 7. *A. cantoniensis* inhibits expression of the four core targets. Bar = 50 μm. Data are expressed as mean ± SD; $^{\#}P < 0.05$ versus control, $^{\#\#}P < 0.01$ versus control, $^{*}P < 0.05$ versus model, $^{**}P < 0.01$ versus model. Note: AC-30: *Abrus cantoniensis*, 30 g/kg.

but also noise[37]. Identifying targets by intersecting different results is considered to be the best means of minimizing significant differences.

To further narrow the anti-hepatic fibrosis targets of *A. cantoniensis*, the targets from the network pharmacology analysis were intersected with those from the proteomics analysis to obtain 14 targets. The importance of the 14 targets was further analyzed using the random forest method and the median value of the PPI network. Four core targets, CDK2, DNMT1, BRAF, and PDGFRB, were identified based on the combined results of the two methods. Studies showed that knocking out CDK2 in hepatic stellate cells improved

the pathological changes characteristic of hepatic fibrosis[38]. DNMT1 regulates hepatic stellate cell activation through multiple pathways by mediating DNA methylation modifications[39]–[40]. BRAF was found to mediate the epithelial mesenchymal transition through MEK1, and inhibition of the transition effectively ameliorated hepatic fibrosis[41]–[42]. Modulation of the PDGFRB signaling pathway, inhibition of hepatic stellate cell proliferation and activation, and promotion of hepatic stellate cell apoptosis were shown to alleviate CCl_4-induced hepatic fibrosis[43]. Licochalcone B arrested the cell cycle by inhibiting CDK2 expression; arrest of the hepatic stellate cell cycle significantly reduced extracellular matrix deposition[38,44]. Hesperetin may also arrest the cell cycle by inhibiting CDK2 expression[45]. Furthermore, studies found that piperine inhibited hepatic stellate cell activation and reduced ECM deposition[46]. Further molecular docking and molecular dynamics simulations of the four core targets revealed that licochalcone B, L-abrine, hesperetin, and piperine, potential active compounds of *A. cantoniensis*, demonstrated strong binding and stable docking with BRAF, CDK2, DNMT1, and PDGFRB, respectively. Immunohistochemistry results showed that *A. cantoniensis* inhibited the expression of the four core targets, consistent with the proteomics results. This further suggested that the four core targets identified here may be the key targets of *A. cantoniensis* in ameliorating hepatic fibrosis.

This study has certain limitations. First, no functional revertant experiments were conducted for the identified key targets to verify the findings of this study. Second, in vitro cellular experiments were not conducted to validate the effects of the potential active compounds of *A. cantoniensis* on the four key targets, which may further elucidate the material basis of the pharmacological actions of *A. cantoniensis*. Additional in vitro cellular studies will be conducted in the future, in which activated hepatic stellate cells are treated with the four potential active compounds. Molecular biology techniques will be used to elucidate the effects of the compounds on the expression of the four key targets, and the regulatory mechanisms governing these critical targets will be investigated. Finally, while the dosage of *A. cantoniensis* used in this study was safe based on the absence of a toxic reaction in vivo and supportive literature, future investigations would benefit from a dedicated OECD-guided toxicity study.

Conclusion

In conclusion, our integrated multi-omics study definitively established *A. cantoniensis* as a multi-target therapy against hepatic fibrosis, with CDK2, DNMT1, BRAF, and PDGFRB as key targets. Molecular docking and dynamics simulations confirmed the strong binding affinity and stability of the key phytochemicals licochalcone B, L-abrine, hesperetin, and piperine with these targets. Immunohistochemical validation confirmed that the expression of these targets was suppressed by these key phytochemicals, supporting the computational predictions. This study deciphered the molecular basis of *A. cantoniensis* efficacy and provided a foundation for developing *A. cantoniensis* into a standardized phytomedicine or a source for novel anti-fibrotic drugs.

Consent to publish All authors have carefully read and revised the full text and agreed to its publication.

Data availability

The data used and analyzed in this study are included within the article.

Received: 23 September 2025; Accepted: 19 December 2025
Published online: 24 December 2025

References

1. Devarbhavi, H. et al. Global burden of liver disease: 2023 update. *J. Hepatol.* **79**, 516–537. https://doi.org/10.1016/j.jhep.2023.03.017 (2023).
2. Bai, Y. et al. Inflammation-responsive cell membrane-camouflaged nanoparticles against liver fibrosis via regulating endoplasmic reticulum stress and oxidative stress. *Adv. Mater.* **36**, e2310443. https://doi.org/10.1002/adma.202310443 (2024).
3. McQuitty, C. E., Williams, R., Chokshi, S. & Urbani, L. Immunomodulatory role of the extracellular matrix within the liver disease microenvironment. *Front. Immunol.* **11** https://doi.org/10.3389/fimmu.2020.574276 (2020).
4. Batudeligen. Luteolin alleviates liver fibrosis in rat hepatic stellate cell HSC-T6: A proteomic analysis. *Drug Des. Devel Ther.* **17**, 1819–1829. https://doi.org/10.2147/DDDT.S402864 (2023).
5. Roehlen, N., Crouchet, E. & Baumert, T. F. Liver fibrosis: Mechanistic concepts and therapeutic perspectives. *Cells* **9** https://doi.org/10.3390/cells9040875 (2020).
6. Wu, E. Y. et al. Optimization of ultrasonic-assisted extraction of total flavonoids from abrus cantoniensis (Abriherba) by response surface methodology and evaluation of its anti-inflammatory effect. *Molecules*. **27**, 2036 (2022). https://doi.org/10.3390/molecules27072036
7. Zhang, G. et al. Abrus cantoniensis hance: Ethnopharmacology, phytochemistry and pharmacology of a promising traditional Chinese medicine. *J. Ethnopharmacol.* **334** https://doi.org/10.1016/j.jep.2024.118543 (2024).
8. Guo, Z. H. et al. Rapid identification of the chemical constituents of abrus cantoniensis by UPLC-Q-TOF/MS technique combined with UNIFI platform. *J. China Pharm.* **33**, 2852–2857. https://doi.org/10.6039/j.issn.1001-0408.2022.23.07 (2022).
9. Lin, X., Zhang, C. & Huang, B. Hepatoprotective action mechanism and quantification of Soyasaponin Bb in Abri herba by HPLC and network pharmacology. *J. Ethnopharmacol.* **337** https://doi.org/10.1016/j.jep.2024.118850 (2025).
10. Xu, C. et al. Protective effects of abrus cantoniensis hance against liver injury through modulation of intestinal microbiota and liver metabolites. *Ecotoxicol. Environ. Saf.* **279** https://doi.org/10.1016/j.ecoenv.2024.116495 (2024).
11. Daina, A., Michielin, O. & Zoete, V. SwissADME: A free web tool to evaluate pharmacokinetics, drug-likeness and medicinal chemistry friendliness of small molecules. *Sci. Rep.* **7** https://doi.org/10.1038/srep42717 (2017).
12. Singh, Y., Jajoriya, A. K. & Kanojiya, S. Exploring the pharmacological effect of cardiac glycosides against hepatocellular carcinoma using network pharmacology. *Pharmacol. Res. Nat. Prod.* **8** https://doi.org/10.1016/j.prenap.2025.100307 (2025).
13. Stelzer, G. et al. The GeneCards suite: From gene data mining to disease genome sequence analyses. *Curr. Protoc. Bioinf.* **54**, 1.30.1–1.30.33 (2016). https://doi.org/10.1002/cpbi.5
14. Amberger, J. S., Bocchini, C. A., Scott, A. F. & Hamosh, A. OMIM.org: Leveraging knowledge across phenotype-gene relationships. *Nucleic Acids Res.* **47**, D1038–D. https://doi.org/10.1093/nar/gky1151 (2019).

15. Chen, X., Ji, Z. L. & Chen, Y. Z. T. T. D. Therapeutic target database. *Nucleic Acids Res.* **30**, 412–415. https://doi.org/10.1093/nar/30.1.412 (2002).
16. Szklarczyk, D. et al. The STRING database in 2023: Protein-protein association networks and functional enrichment analyses for any sequenced genome of interest. *Nucleic Acids Res.* https://doi.org/10.1093/nar/gkac1000 (2023). .51,D638-D646.
17. Shannon, P. et al. Cytoscape: A software environment for integrated models of biomolecular interaction networks. *Genome Res.* **13**, 2498–2504. https://doi.org/10.1101/gr.1239303 (2003).
18. Kim, S. et al. PubChem 2025 update. *Nucleic Acids Res.* **53** (D1516-D1525). https://doi.org/10.1093/nar/gkae1059 (2025).
19. Pundir, S., Martin, M. J. & O'Donovan, C. & UniProt, Consortium. UniProt Tools. Curr. Protoc. Bioinformatics. **53**, 1.29.1–1.29.15 (2016). https://doi.org/10.1002/0471250953.bi0129s53
20. Hu, Y. et al. Astragaloside IV prevents liver fibrosis by blocking glycolysis-mediated macrophage M1 polarization. *Eur. J. Pharmacol.* **995** https://doi.org/10.1016/j.ejphar.2025.177353 (2025).
21. Mohammed, O. S., Attia, H. G., Mohamed, B. M. S. A., Elbaset, M. A. & Fayed, H. M. Current investigations for liver fibrosis treatment: between repurposing the FDA-approved drugs and the other emerging approaches. *J. Pharm. Pharm. Sci.* **26**, 11808. https://doi.org/10.3389/jpps.2023.11808 (2023).
22. Liang, C., Liu, J., Jiang, M., Zhu, Y. & Dong, P. The advancement of targeted regulation of hepatic stellate cells using traditional Chinese medicine for the treatment of liver fibrosis. *J. Ethnopharmacol.* **341** https://doi.org/10.1016/j.jep.2024.119298 (2025).
23. Liang, X. et al. Abrine, an IDO1 inhibitor, suppresses the immune escape and enhances the immunotherapy of anti-PD-1 antibody in hepatocellular carcinoma. *Front. Immunol.* **14** https://doi.org/10.3389/fimmu.2023.1185985 (2023).
24. Dong, S. et al. Mechanisms of CCl_4-induced liver fibrosis with combined transcriptomic and proteomic analysis. *J. Toxicol. Sci.* **41**, 561–572. https://doi.org/10.2131/jts.41.561 (2016).
25. Ou, Q. et al. Silybin alleviates hepatic steatosis and fibrosis in NASH mice by inhibiting oxidative stress and involvement with the Nf-κB pathway. *Dig. Dis. Sci.* **63**, 3398–3408. https://doi.org/10.1007/s10620-018-5268-0 (2018).
26. Shen, Y. et al. Discrimination of abrus cantoniensis hance and abrus mollis hance using UPLC-Q/TOF-MS and assessment of their in vivo hepatoprotective effects. *J. Ethnopharmacol.* **337** https://doi.org/10.1016/j.jep.2024.118864 (2025).
27. Lin, L. et al. Ginsenoside Rb1 induces hepatic stellate cell ferroptosis to alleviate liver fibrosis via the BECN1/SLC7A11 axis. *J. Pharm. Anal.* **14** https://doi.org/10.1016/j.jpha.2023.11.009 (2024).
28. Zhang, C. et al. Oroxylin A prevents angiogenesis of LSECs in liver fibrosis via Inhibition of YAP/HIF-1α signaling. *J. Cell. Biochem.* **119**, 2258–2268. https://doi.org/10.1002/jcb.26388 (2018).
29. Feng, X. et al. Yinchen gongying decoction mitigates CCl_4-induced chronic liver injury and fibrosis in mice implicated in inhibition of the FoxO1/TGF-β1/ Smad2/3 and YAP signaling pathways. *J. Ethnopharmacol.* **327**, 117975(2024). https://doi.org/10.1016/j.jep.2025.120101
30. Tan, S. et al. Fas/FasL mediates NF-κBp65/PUMA-modulated hepatocytes apoptosis via autophagy to drive liver fibrosis. *Cell. Death Dis.* **12** https://doi.org/10.1038/s41419-021-03749-x (2021).
31. Zhang, M. et al. Hepatic stellate cell senescence in liver fibrosis: Characteristics, mechanisms and perspectives. *Mech. Ageing Dev.* **199** https://doi.org/10.1016/j.mad.2021.111572 (2021).
32. Zuo, L. et al. PI3-kinase/Akt pathway-regulated membrane transportation of acid-sensing ion channel 1a/Calcium ion influx/endoplasmic reticulum stress activation on PDGF-induced HSC activation. *J. Cell. Mol. Med.* **23**, 3940–3950. https://doi.org/10.1111/jcmm.14275 (2019).
33. Wang, F. et al. Canonical Wnt signaling promotes HSC Glycolysis and liver fibrosis through an LDH-A/HIF-1α transcriptional complex. *Hepatology* **79**, 606–623. https://doi.org/10.1097/HEP.0000000000000569 (2024).
34. Wan, J. et al. LC3-associated phagocytosis protects against inflammation and liver fibrosis via immunoreceptor inhibitory signaling. *Sci. Transl. Med.* **12**, eaaw8523. https://doi.org/10.1126/scitranslmed.aaw8523 (2020).
35. Wang, L., Wang, Y. & Quan, J. Exosomes derived from natural killer cells inhibit hepatic stellate cell activation and liver fibrosis. *Hum. Cell.* **33**, 582–589. https://doi.org/10.1007/s13577-020-00371-5 (2020).
36. Li, Y. et al. Integrated network pharmacology, proteomics, molecular docking, and experiments in vivo and in vitro to explore the efficacy and potential mechanism of Bufalin against hepatocellular carcinoma angiogenesis. *J. Ethnopharmacol.* **345** https://doi.org/10.1016/j.jep.2025.119589 (2025).
37. Zhang, P. et al. Network pharmacology: Towards the artificial intelligence-based precision traditional Chinese medicine. *Brief. Bioinform.* **25** https://doi.org/10.1093/bib/bbad518 (2023). ,bbad518.
38. Otto, J. et al. Expression of Cyclin E1 in hepatic stellate cells is critical for the induction and progression of liver fibrosis and hepatocellular carcinoma in mice. *Cell. Death Dis.* **14** https://doi.org/10.1038/s41419-023-06077-4 (2023).
39. Pan, X. Y. et al. Methylation of RCAN1.4 mediated by DNMT1 and DNMT3b enhances hepatic stellate cell activation and liver fibrogenesis through Calcineurin/NFAT3 signaling. *Theranostics* **9**, 4308–4323. https://doi.org/10.7150/thno.32710 (2019).
40. Zhu, H. et al. Sennoside A prevents liver fibrosis by binding DNMT1 and suppressing DNMT1-mediated PTEN hypermethylation in HSC activation and proliferation. *FASEB J.* **34**, 14558–14571. https://doi.org/10.1096/fj.202000494RR (2020).
41. Xie, C. et al. Identification of a BRAF/PA28γ/MEK1 signaling axis and its role in epithelial-mesenchymal transition in oral submucous fibrosis. *Cell. Death Dis.* **13**, 701. https://doi.org/10.1038/s41419-022-05152-6 (2022).
42. Zhang, L., Zhang, Y., Chang, X. & Zhang, X. Imbalance in mitochondrial dynamics induced by low PGC-1α expression contributes to hepatocyte EMT and liver fibrosis. *Cell. Death Dis.* **11** https://doi.org/10.1038/s41419-020-2429-9 (2020).
43. Wang, R. et al. Gomisin D alleviates liver fibrosis through targeting PDGFRβ in hepatic stellate cells. *Int. J. Biol. Macromol.* **235** https://doi.org/10.1016/j.ijbiomac.2023.123639 (2023).
44. Yu, L. et al. Licochalcone B arrests cell cycle progression and induces apoptosis in human breast cancer MCF-7 cells. *Recent. Pat. Anticancer Drug Discov.* **11**, 444–452. https://doi.org/10.2174/1574892811666160906091405 (2016).
45. Wei, L. et al. Effects of Hesperetin on platelet-derived growth factor-BB-induced pulmonary artery smooth muscle cell proliferation. *Mol. Med. Rep.* **13**, 955–960. https://doi.org/10.3892/mmr.2015.4625 (2016).
46. Abdelhamid, A. M., Selim, A. & Zaafan, M. A. The hepatoprotective effect of Piperine against Thioacetamide-Induced liver fibrosis in mice: the involvement of miR-17 and TGF-β/Smads pathways. *Front. Mol. Biosci.* **8**, 754098. https://doi.org/10.3389/fmolb.2021.754098 (2021).

Acknowledgements

We thank the Guangxi University of Chinese Medicine (Guangxi, China) for providing laboratory equipment and technological support. We also acknowledge the linguistic assistance provided by LetPub (www.letpub.com.cn) during the preparation of this paper.

Author contributions

Yang Zheng and Jiahui Wang were responsible for conducting the experiments and drafting the initial manuscript; Liang Liang handled the visualization of figures; Yaxuan Qin managed the data collection; Lei Wang and Huaye Xiao oversaw the experimental design and manuscript revisions.

Funding
This study was funded by the Guangxi Natural Science Foundation (Grant Nos.2024GXNSFAA010235, 2025GXNSFAA069460), the Key Laboratory of Faculty of Chinese Medicine Science Guangxi University of Chinese Medicine (No.02: Fundamental Research on the Prevention and Treatment of Chronic Liver Disease Using Traditional Chinese Medicine and Zhuang-Yao Medicine), the Research Project of Faculty of Chinese Medicine Science Guangxi University of Chinese Medicine (Grant Nos.2024ZZA003,2024ZZA002, 2024ZZB007 and 2024ZZB010), the National Natural Science Foundation of China (Grant No. 82204755), the Guangxi Zhuangyao Pharmaceutical Key Laboratory (Grant No. GXZYYKF2023-05), the Guangxi University of Chinese Medicine Key Program (Grant No. 2024ZD007), and the National Student Innovation and Entrepreneurship Training Programme of Faculty of Chinese Medicine Science Guangxi University of Chinese Medicine (Grant No. 202513643004).

Declarations

Competing interests
The authors declare no competing interests.

Additional information
Supplementary Information The online version contains supplementary material available at https://doi.org/10.1038/s41598-025-33640-0.

Correspondence and requests for materials should be addressed to L.W.

Reprints and permissions information is available at www.nature.com/reprints.

Publisher's note Springer Nature remains neutral with regard to jurisdictional claims in published maps and institutional affiliations.